Eur. J. Mineral., 37, 1–12, 2025
https://doi.org/10.5194/ejm-37-1-2025

European Journal of Mineralogy
Open Access

Insights from the compositional evolution of a multi-coloured, zoned tourmaline from the Cruzeiro pegmatite, Minas Gerais, Brazil

Giovanni B. Andreozzi[1,2], Claudia Gori[3], Henrik Skogby[4], Ulf Hålenius[4], Alessandra Altieri[1], and Ferdinando Bosi[1,2]

[1]Department of Earth Sciences, Sapienza University of Rome, Piazzale Aldo Moro, 5, 00185 Rome, Italy
[2]CNR–IGAG c/o Department of Earth Sciences, Sapienza University of Rome, Piazzale Aldo Moro, 5, 00185 Rome, Italy
[3]independent researcher: Largo Gaetano De Sanctis, 7, 00179 Rome, Italy
[4]Department of Geosciences, Swedish Museum of Natural History, P.O. Box 50007, 10405 Stockholm, Sweden

Correspondence: Giovanni B. Andreozzi (gianni.andreozzi@uniroma1.it)

Received: 28 August 2024 – Revised: 24 October 2024 – Accepted: 25 October 2024 – Published: 6 January 2025

Abstract. This study compares the compositional evolution of a multi-coloured, zoned tourmaline crystal from the Cruzeiro pegmatite, Brazil, with the compositions of homogeneous tourmaline crystals systematically collected from the outer to the inner zones of the same pegmatite. Four representative fragments of the multi-coloured, zoned tourmaline were thoroughly investigated using single-crystal X-ray diffraction; electron microprobe analysis; and ^{57}Fe Mössbauer, Fourier transform infrared, and optical absorption spectroscopies to obtain the full composition and site occupancies. The fragments are classified, from core to rim, as ^{W}O-rich, F-bearing schorl (black inner and outer core) and Fe^{2+}-rich, ^{W}OH-bearing fluor-elbaite (blue inner and green outer rim). A negative correlation between F and Fe^{2+} contents was evidenced, approximated by the equation $F = 1 - 0.33Fe^{2+}$ (in atoms per formula unit) and consistent with the observed tourmaline evolution from schorl to fluor-elbaite.

The evolution trend from core to rim mirrors the compositional variation exhibited by the homogeneous tourmaline crystals collected across the Cruzeiro pegmatite, from the border zone to the intermediate zone. This shows that the chemical variations in a zoned tourmaline, observed at the scale of single crystals, record not only its crystal growth history, but also the chemical evolution of the host pegmatite. Moreover, in uncontaminated granitic pegmatite systems such as that of Cruzeiro, the compositional evolution of tourmaline progresses from schorl to fluor-elbaite, rather than from schorl to elbaite, to reflect co-enrichment in Li and F during fractional crystallization.

1 Introduction

Granitic pegmatites are strategically relevant because they host a variety of rare-element-bearing minerals and contain most of the world reserves of these elements (Gysi and Williams-Jones, 2013; Shaw et al., 2016). Different hypotheses have been proposed to explain how pegmatite-forming melts are generated, although pegmatites may be classified regardless of the mechanism of formation (Martin and De Vito, 2005; London, 2005, 2014; Simmons and Webber, 2008; Černý et al., 2012; Novák et al., 2012; Shaw et al., 2016; London, 2018). Pegmatites enriched in incompatible elements (high-field-strength and large-ion lithophile elements) belong to the rare-element (REL) class, and among them a particularly important subclass is that of REL enriched in Li, in turn affiliated to the LCT (Li–Cs–Ta) family (Černý, 1991; Černý and Ercit, 2005; Černý et al., 2012; Linnen et al., 2012).

In the area of Governador Valadares, Minas Gerais, Brazil, hundreds of pegmatites occur, being emplaced from

syn-tectonic fractional crystallization of granitic magma at 582 Ma (de Mello and Bilal, 2012). The mineral assemblage indicates that the pegmatites crystallized at temperatures ranging from 360 to 570 °C and at pressures ranging from 1.1 to 3 kbar (Bilal et al., 1997, 1998). Boron isotope analysis measured on tourmaline crystals that come from an area south of Governador Valadares yielded δ^{11}B values in the range of −16.3 ‰ to −11.3 ‰ for the pegmatites, −13.8 ‰ to −11.5 ‰ for the host schists of the São Tomé Formation, and −14.0 ‰ to −13.1 ‰ for the tourmaline-bearing facies of Córrego do Onça that belong to the Urucum suite, suggesting a common source for all the analysed rocks (Lima et al., 2019). The granitic pegmatite of Cruzeiro (located north of Governador Valadares, close to the small village of São Josè da Safira) is an LCT pegmatite that consists of three sub-vertical, parallel, symmetrically zoned dikes intruded in the quartzite of the Serra da Safira Sequence, and it is an excellent example of a pegmatite body where the pegmatitic melt–fluid system crystallized virtually without any chemical interaction with the surrounding host rock. The three dikes of the Cruzeiro may be derived from a granitic pluton (although granite was not found nearby), and their emplacement seems to have been controlled by regional structure, as indicated by the concentration of many other pegmatitic bodies in the surrounding area along lineaments oriented N10–20° W (César-Mendes, 1995). The Cruzeiro pegmatite is world-famous for having produced a large quantity of gigantic and beautiful tourmaline crystals, ranging in size from centimetres to decimetres and exhibiting a variety of colours and chemical compositions (Bilal et al., 1997, 1998; Federico et al., 1998).

Tourmaline is well known as a valuable indicator of chemical changes in crystallization environments and of physical conditions, in particular temperature, and the retention of that information over time has led to the concept of tourmaline being a "geologic DVD", even on the scale of single crystals (e.g. Dutrow and Henry, 2011; van Hinsberg et al., 2011; Lussier et al., 2011; Lussier and Hawthorne, 2011). A comprehensive survey of tourmaline compositional variation across the Cruzeiro dikes was made by Federico et al. (1998), and representative samples belonging to the dravitic–schorlitic–elbaitic series were investigated by Bosi and Lucchesi (2004), Bosi et al. (2005, 2015), Andreozzi et al. (2008), and Skogby et al. (2012). Previous studies found that tourmaline is abundant in border, wall, and intermediate zones of the pegmatite and that its chemical composition varies, from outer to inner zones, from Mg-bearing schorl to schorl to elbaite. In detail, schorl and elbaite may show ^{W}(O, OH, F) at the $O1$ site according to the main substitutional mechanism $Fe^{2+} + Fe^{3+} + O \rightarrow Li + Al + (OH + F)$. Furthermore, the fluor-elbaite from Cruzeiro was recognized as a new mineral species by Bosi et al. (2013).

At Cruzeiro, due to the absence of contamination with the quartzite host rock, it was reasonable to assume that the evolution of both tourmaline composition and its paragenesis reflected the physico-chemical evolution of the pegmatitic melt (Federico et al., 1998; Bosi et al., 2005). Chemical evolution of the Cruzeiro tourmaline composition is highlighted by the colour shown by the homogeneous crystals, which varies from black in the schorl crystals occurring in the outer zones to blue and green in the elbaite crystals occurring in the inner zones of the pegmatite (Federico et al., 1998). In addition, single crystals showing distinctly colour-zoned schemes (black–blue, black–green, blue–green, or even green–pink) are occasionally observed in the inner zones of the Cruzeiro dikes. In these crystals, colour zoning is commonly horizontal relative to the c axis (i.e. concentric), but it may also be vertical, following the tourmaline prismatic growth. Furthermore, distinct colour change (from dark blue to yellowish olive green) was observed in three different generations of fibrous tourmalines hosted in a pink elbaite crystal (Dutrow and Henry, 2000). More rarely, within inner zones there is the occurrence of multi-coloured, zoned single crystals that show a colour sequence mirroring the colour sequence exhibited by the homogeneous tourmaline crystals occurring across the pegmatite, from outer to inner zones. This last observation leads to the hypothesis that at Cruzeiro, the variable composition of multi-coloured, zoned tourmaline single crystals may have recorded the melt chemical evolution during the pegmatite differentiation.

To test this hypothesis, selected fragments of a multi-coloured tourmaline crystal were examined in detail using an integrated approach, which includes single-crystal X-ray diffraction and structure refinement, electron microprobe analysis, Mössbauer spectroscopy, Fourier transform infrared spectroscopy, and optical absorption spectroscopy.

2 Materials and methods

2.1 Cruzeiro pegmatite internal zoning and tourmaline sample occurrence

The Cruzeiro pegmatite is a Li-, Be-, B-, Nb-, Ta-, and Zn-enriched miarolitic pegmatite located near the municipality of São José da Safira, Governador Valadares, Minas Gerais, Brazil. The granitic pegmatite is included in a metamorphic series of Proterozoic age known as the schist–quartzite sequence. This sequence crops out with thick layers of coarse-grained quartzite containing the lens-shaped dikes of the Cruzeiro pegmatite (Bilal et al., 1997, 1998; Federico et al., 1998). The Cruzeiro pegmatite consists of three sub-vertical, parallel dikes, showing sharp boundaries with the host quartzite. Dike 1 is 1300 m long and up to 60 m wide; dike 2 is 900 m long and about 20 m wide; dike 3 is 700 m long and 8 m wide. The three dikes show clear horizontal zoning and perfect symmetrical development around a quartz core (Fig. 1a). The zoning description includes a border zone, a wall zone, and an intermediate zone, locally divided into external, medium, and internal. The different zones are defined by relative abundance of coexisting min-

eral assemblages: in the outer zones (border and wall zones), there is the occurrence of quartz, K-feldspar, muscovite, black schorl, prismatic blue beryl, almandine-rich garnet, and columbite–tantalite (Nb > Ta); in the inner zones (intermediate zone), there is the occurrence of Li-bearing mica, quartz, platy albite (cleavelandite), multi-colour elbaite, tabular pink beryl, spodumene, spessartine-rich garnet, amblygonite, Mn-apatite, tantalite–columbite (Ta > Nb), gahnite, and cassiterite. Tourmaline crystals are ubiquitous but are particularly abundant in the wall and intermediate zones as well as in the miarolitic pockets that are randomly distributed around the quartz core (Bilal et al., 1997, 1998; Federico et al., 1998).

The tourmaline sample under investigation is from the intermediate zone of dike 3 and is a prismatic, multi-colour-zoned single crystal, ca. 8 cm wide and 10 cm long. The prismatic crystal exhibits an evident horizontal zonation relative to the c axis, like many other crystals from the same pegmatite. The sample under investigation exhibits a large homogeneous black core in sharp contact with a narrow blue inner rim, which in turn shows clear contact with a green outer rim (Fig. 1b, c). Four homogeneous fragments of millimetre size were extracted from the crystal, and they are representative of the green outer rim (T1), the blue inner rim (T2), the black outer core (T3), and the black inner core (T4). The vividly coloured crystal fragments are of gem quality (Fig. 2). Fragment T3 and partly fragments T1 and T2 were previously investigated by Bosi et al. (2015).

2.2 ^{57}Fe Mössbauer spectroscopy

The selected fragments were powdered in an agate mortar under acetone; then the Mössbauer absorber was prepared by pressing the finely ground powder with an acrylic resin into a self-supporting disc (1.0 cm diameter). To obtain an absorber with an Fe thickness of $\sim 4\,\mathrm{mg\,cm^{-2}}$, the amount of tourmaline used to make the absorber varied from 40 to 100 mg, depending on the chemical composition. Several ^{57}Fe Mössbauer spectra were collected at room temperature in transmission mode using a conventional constant-acceleration spectrometer with a ^{57}Co source of 0.99 GBq (25 mCi) in a 7 mm Rh matrix. Data collection time was up to 5 d to attain optimal statistics. Spectral data for the velocity range $\pm 4\,\mathrm{mm\,s^{-1}}$ were recorded in a multi-channel analyser using 512 channels. Results were calibrated against a foil (0.025 mm thick) of high-purity α-Fe, and raw data were folded to form 256 channels. Each spectrum was fitted assuming Lorentzian peak shapes using the Recoil 1.04 fitting program (Lagarec and Rancourt, 1998). To obtain the best fit (evaluated using the reduced χ^2 parameter), several fitting models with unconstrained hyperfine parameters were tried. The best fitting model consisted of four doublets for ferrous iron with unconstrained centre shift (δ), quadrupole splitting (ΔE_Q), and peak width (Γ) parameters and one doublet for ferric iron with fixed δ and ΔE_Q. Uncertainties were calculated using the covariance matrix and estimated at $\pm 0.02\,\mathrm{mm\,s^{-1}}$ for δ, ΔE_Q, and Γ and at $\sim \pm 3$ % for absorption areas. A representative absorption spectrum is shown in Fig. S1 in the Supplement, and the hyperfine parameters of fitted spectra are reported in Table S1 in the Supplement. These data reveal that the Fe^{3+}/Fe_{TOT} ratio for all fragments is zero or very close to zero (within experimental error).

2.3 Single-crystal structural refinement (SREF)

X-ray diffraction data from the selected crystal fragments were acquired on a Bruker KAPPA APEX II single-crystal diffractometer equipped with a CCD area detector ($6.2 \times 6.2\,\mathrm{cm^2}$ active detection area, 512×512 pixels) and a graphite crystal monochromator, using Mo$K\alpha$ radiation from a fine-focus sealed X-ray tube. The sample-to-detector distance was 4 cm. A total of 3265 exposures (step = 0.2°, time per step = 20 s) were collected, and a completeness of about 95 % was achieved. Unit-cell parameters were refined using the Bruker AXS SAINT program on reflections with $I > 10\sigma_I$ in the range $6° < 2\theta < 74°$. The intensity data were processed and corrected for Lorentz, polarization, and background effects with APEX2 software program of Bruker AXS. The data were corrected for absorption using the multi-scan method (SADABS). The absorption correction led to a significant improvement in R_{int}. No violations of $R3m$ symmetry were noted.

Structure refinement was performed with the SHELXL2013 program (Sheldrick, 2015). Starting coordinates were taken from Bosi et al. (2015). The scale factor, the extinction coefficient, atom coordinates, site-scattering values, and atom-displacement factors were the variable parameters. In detail, the X site was modelled using the Na scattering factor, the Y site was modelled considering the presence of Li versus Fe (for samples T1 and T2) and Al versus Fe (for sample T4), and the Z site was modelled considering the presence of Al (for samples T1 and T2) and Fe versus Al (for sample T4). The T and B sites were modelled with Si and B scattering factors, respectively, and with a fixed occupancy of 1 because refinement with unconstrained occupancies showed no significant deviations from this value. The $O1$ site was refined with occupancies of O and F fixed to the value of the structural formula. The position of the H atom bonded to the oxygen at the $O3$ position in the structure was taken from the difference Fourier map and incorporated into the refinement model; the $O3$–$H3$ bond lengths were constrained to be 0.97(3) Å. Three full-matrix refinement cycles with isotropic-displacement parameters for all atoms were followed by anisotropic cycles until convergence was attained. There were no significant correlations over 0.7 between the parameters at the end of refinement. Table S2 lists crystal data, data-collection information, and refinement details; Table S3 gives the fractional atom coordinates and equivalent-displacement

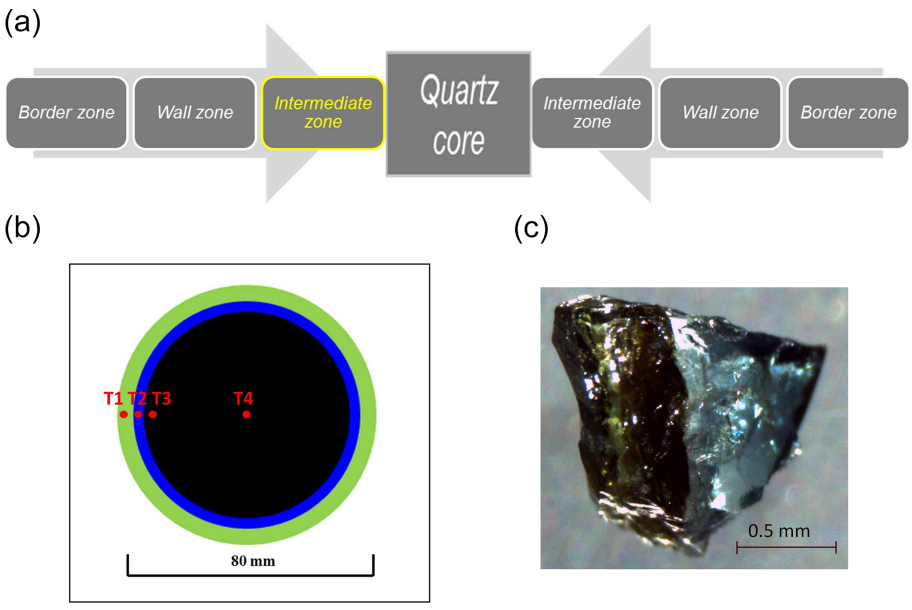

Figure 1. **(a)** Internal zoning of the Cruzeiro pegmatite. The multi-coloured, zoned tourmaline crystal investigated occurred on the left-hand side of the internal intermediate zone. **(b)** Simplified representation of the multi-coloured zoning in the tourmaline crystal investigated here. From rim to core: T1, green outer rim; T2, blue inner rim; T3, black outer core; T4, black inner core. **(c)** Tourmaline rim fragment showing the sharp contact between the blue and the green portions.

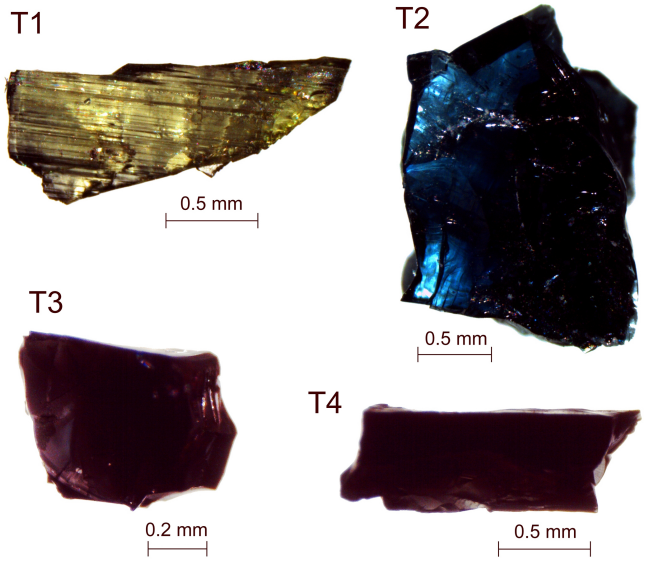

Figure 2. Selected fragments extracted from the multi-coloured, zoned tourmaline crystal from the Cruzeiro pegmatite. From rim to core: T1, green outer rim; T2, blue inner rim; T3, black outer core; T4, black inner core.

parameters; and Table S4 gives selected bond distances and mean atomic numbers (m.a.n.'s).

2.4 Electron microprobe (EMP) analysis

The chemical composition of the selected tourmaline fragments used for SREF analysis was obtained by electron microprobe. A wavelength-dispersive spectroscopy (WDS) mode with a Cameca SX50 instrument operating at an accelerating potential of 15 kV, a sample current of 15 nA, and 10 µm beam diameter was used. Reference standards were minerals and synthetic compounds: wollastonite (Si, Ca), magnetite (Fe), rutile (Ti), corundum (Al), vanadinite (V), fluorphlogopite (F), periclase (Mg), jadeite (Na), K-feldspar (K), sphalerite (Zn), metallic Cr, Mn, and Cu. The PAP routine was applied (Pouchou and Pichoir, 1991). The oxide weight percent of V, Cr, and Cu was below the detection limit (0.02 wt %). For each fragment, mean values of 10 spot analyses are reported in Table 1.

2.5 Fourier transform infrared (FTIR) absorption spectroscopy

The tourmaline fragment T4 was measured by FTIR spectroscopy to characterize the OH vibrational bands (Fig. S2). A Bruker Equinox 55 spectrometer with a Bio-Rad infrared microscope, operating with a Globar source, a KBr beam splitter, a wire-grid polarizer, and an MCT (mercury–cadmium–telluride) detector, was used. Polarized spectra parallel to and perpendicular to the crystallographic *c*-axis

Table 1. Chemical composition of selected fragments of a multi-coloured, zoned tourmaline crystal from the Cruzeiro pegmatite (Minas Gerais, Brazil).

	T1	T2	T3*	T4
SiO_2 wt %	37.32(17)	36.34(9)	34.71(19)	35.58(21)
TiO_2	0.06(2)	0.08(2)	0.30(3)	0.30(1)
B_2O_3[a]	10.80	10.64	10.27	10.38
Al_2O_3	37.27(16)	36.40(25)	34.07(13)	33.41(6)
Fe_2O_3[b]	–	–	0.47	0.53
FeO[b]	5.81	8.11	13.77	11.35
MnO	1.13(9)	1.48(7)	0.38(10)	0.16(6)
MgO	0.10(1)	0.17(3)	0.72(4)	2.80(3)
ZnO	0.09(5)	0.19(9)	0.41(6)	0.22(5)
CaO	0.12(2)	0.15(1)	0.10(2)	0.14(1)
Na_2O	2.69(7)	2.49(6)	1.99(6)	2.07(5)
K_2O	0.03(1)	0.04(1)	0.06(1)	0.05(1)
Li_2O[c]	1.47	1.01	–	–
F	1.35(14)	1.18(13)	0.52(12)	0.40(10)
H_2O[d]	3.07	3.03	2.96	3.04
$-O\equiv F$	−0.57	−0.50	−0.22	−0.17
Total	100.75	100.83	100.50	100.25
FeO_{EMP}	5.81(15)	8.11(24)	14.19(20)	11.82(16)
Atomic fractions				
Si apfu	6.004	5.937	5.870	5.961
Ti^{4+}	0.008	0.010	0.040	0.038
B	3.000	3.000	3.000	3.000
Al	7.065	7.009	6.790	6.596
Fe^{3+}	–	–	0.060	0.066
Fe^{2+}	0.782	1.108	1.950	1.590
Mn	0.154	0.205	0.050	0.023
Mg	0.025	0.041	0.180	0.700
Zn	0.011	0.023	0.050	0.027
Ca	0.020	0.027	0.020	0.026
Na	0.838	0.789	0.650	0.672
K	0.006	0.009	0.010	0.010
Li	0.952	0.667	–	–
F	0.687	0.612	0.280	0.211
OH	3.291	3.300	3.340	3.395

Errors for oxides and F (in brackets) are the standard deviations of 10 analyses. Atomic fractions are normalized to 31 anions (O, OH, F); apfu denotes atoms per formula unit. * Data from Bosi et al. (2015). [a] Calculated by stoichiometry, assuming 3 B apfu (see text). [b] Determined by Mössbauer spectroscopy. [c] Calculated by stoichiometry and IR information (see text). [d] Calculated by bond valence relation (see text).

direction of the T4 sample were acquired in the wavenumber range 2000–8000 cm^{-1} with a resolution of 2 cm^{-1} using a rectangular measurement area of ∼ 50 µm × 50 µm. The doubly polished crystal plate had a thickness of 42 µm. The fragments T1, T2, and T3 had previously been studied using the same methodological approach, and the spectra are published in Bosi et al. (2015).

2.6 Optical absorption spectroscopy (OAS)

Polarized optical absorption spectra of the tourmaline fragments T1, T2, and T4 were recorded at room temperature in the spectral range 270–1100 nm (37 037–9091 cm^{-1}) on double-sided (100 µm) polished single-crystal sections. The spectral resolution was 1 nm using an AvaSpec-ULS2048x16 spectrometer attached via a 400 µm UV fibre cable to a Zeiss Axiotron UV microscope. The light source was a 75 W xenon arc, and Zeiss Ultrafluar 10× lenses served as the objective and condenser. The size of the circular measuring aperture was 64–200 µm in diameter. The polarizer was a UV-quality Glan–Thompson prism with a working range from 250 to 2700 nm (40 000 to 3704 cm^{-1}). The wavelength scale of the spectrometer was calibrated against standards doped with Ho_2O_3 and Pr_2O_3/Nd_2O_3 (Hellma glass filters 666F1 and 666F7). The accuracy was better than 15 cm^{-1} in the wavelength range 300–1100 nm. A Bruker Equinox 55 FTIR spectrometer equipped with a halogen lamp source, a CaF_2 beam splitter, a wire-grid polarizer, and an InSb detector was used to collect the polarized near-infrared spectra. The samples were masked by a circular aperture of 64–200 µm diameter, and a total of 512 scans were acquired over the spectral range 2000–13 000 cm^{-1} at a resolution of 4 cm^{-1}. The UV–Vis–NIR spectra were fitted using the PeakFit 4.12 software (Jandel) assuming Gaussian peak shapes and are shown in Fig. S3. The fragment T3 had previously been studied using the same methodological approach, and the spectra are published in Bosi et al. (2015).

3 Results

Tourmaline is a mineral characterized by an intermediate structural complexity (100–500 bit per unit cell; Krivovichev, 2013). Nonetheless, for an effective classification to be accomplished, actual contents of H, Li, B, Fe^{2+}, and Fe^{3+} need to be quantified or at least well constrained. In the present case, Fe^{2+} and Fe^{3+} proportions were quantified via ^{57}Fe Mössbauer spectroscopy and H, Li, and B were estimated exploiting the well-tested multi-analytical approach based on the integrated combination of structural, chemical, and spectroscopic data, which gave excellent results on tourmaline and other borosilicates (e.g. Andreozzi et al., 2000, 2004, 2008; Bosi et al., 2013, 2015, 2018).

3.1 FTIR and OAS results

FTIR spectra of fragment T4 recorded in polarized mode perpendicular and parallel to the *c* axis are reported in Fig. S2 and consist of a set of absorption bands with different intensities in the OH-stretching region (3300–3800 cm^{-1}). The absorption bands in the *c*-axis direction are strongly polarized, as previously noticed in polarized-FTIR studies on tourmalines (e.g. Gebert and Zemann, 1965). Unfortunately, it was not possible to thin the sample sufficiently to avoid off-scale absorption intensity for the strongest bands.

The ^{O1}OH stretching modes are affected by the *X*-site constituents, with the bands of ∼ 3600–3700 cm^{-1} normally assigned to $^{X}\square$, whereas bands above 3700 cm^{-1} are consid-

ered to be associated with ^{X}Na (e.g. Gonzalez-Carreño et al., 1988; Berryman et al., 2016). The two absorption peaks at 3630–3643 cm^{-1} are probably related to the atomic arrangement ^{Y}(Fe,Fe,Al)–^{O1}OH–$^{X}\square$, in agreement with Gonzalez-Carreño et al. (1988) and Watenphul et al. (2016). Their intensities decrease from the inner core to outer rim (T4 → T1), and this is consistent with a corresponding decrease in Fe^{2+} content (Table 1). Comparing the spectra of T4 with those of T1, T2, and T3 published in Bosi et al. (2015), the peaks at 3670–3682 cm^{-1} are clearly evident in the T1 fragment and disappear in T3 and T4. These peaks are related to Li content and can be assigned to the atomic arrangement ^{Y}(Al,Al,Li)–^{O1}OH–$^{X}\square$ (Gonzalez-Carreño et al., 1988). Moreover, the peak at ∼ 3720 cm^{-1} becomes evident only in the T4 fragment and can be assigned to the atomic arrangement ^{Y}(Fe,Fe,Al)––^{O1}OH–^{X}Na (Watenphul et al., 2016).

The optical spectra in the UV–Vis–NIR region of the T4, T2, and T1 crystal fragments are reported in Fig. S3. Spectra recorded in polarized mode perpendicular to the *c*-axis direction (E ∥ *a*) show two main strong absorption bands at ∼ 13 800 and ∼ 9000 cm^{-1} that are due to Fe^{2+} absorption (e.g. Mattson and Rossman, 1987). An additional broad band can be observed in the range of 24 000–23 000 cm^{-1} ascribable to Fe^{2+}–Ti intervalence charge-transfer (IVCT) transitions (e.g. Mattson and Rossman, 1987). A weak absorption band at ∼ 18 000 cm^{-1}, only visible in the T4 fragment, can be instead ascribed to Fe^{2+}–Fe^{3+} IVCT transitions (e.g. Mattson and Rossman, 1987).

A comparison of the OAS spectra of the crystal fragments (including T3, previously published in Bosi et al., 2015) reveals a decrease in the intensity of the bands at ∼ 13 800 and ∼ 9000 cm^{-1}, consistent with a corresponding decrease in the Fe^{2+} content from core to rim (T4 → T1) (Table 1). Moreover, the strong polarization of the ∼ 13 800 and 9000 cm^{-1} absorption band in the T4 and T3 crystal fragments, as well as the occurrence of the ∼ 18 000 cm^{-1} band, is attributable to the presence of minor Fe^{3+}, in agreement with Mössbauer analysis (Table S1).

In the four crystal fragments, the position of the Fe^{2+}–Ti IVCT band shows a significant variation, being shifted from ∼ 23 000 cm^{-1} in the T4, T3, and T2 fragments to ∼ 24 000 cm^{-1} in the T1 fragment (Fig. S3). Additionally, the intensity of this band seems not to be related to the Ti and Fe^{2+} contents, which decrease from core to rim. The shift to high energy of the Fe^{2+}–Ti IVCT band could be explained by differences in local cation ordering, as previously observed in a tourmaline sample from the island of Elba (Altieri et al., 2022). Indeed, Mössbauer analysis revealed that in the T4, T3, and T2 fragments, a lower percentage of Fe^{2+} occupies the *Y*3 local configuration (in comparison to *Y*1 and *Y*2), while in the T1 fragment Fe^{2+} is approximately equally distributed over the *Y*1, *Y*2, and *Y*3 local configurations (Table S1).

3.2 Atomic fractions and site populations

The chemical composition of the studied tourmaline fragments includes B, the contents of which were assumed to be stoichiometric (i.e. B = 3 atoms per formula unit (apfu)) in agreement with the SREF results. In fact, both the site scattering and the bond-length results of the *B* and *T* sites are consistent with previous studies where the *B* site is fully occupied by B and the *T* site is B-free (e.g. Bosi and Lucchesi, 2007). The Mn oxidation state was assumed to be Mn^{2+} based on OAS results. The OH_{TOT} contents were determined through bond valence analysis using parameters from Brown and Altermatt (1985). This analysis yielded a bond valence sum (BVS) at *O*3 of 1.10–1.15 valence units, which is consistent with ^{V}OH = 3.00 apfu (e.g. Grice and Ercit, 1993). BVSs at *O*1 were 0.81, 0.87, 1.13, and 1.16 valence units for samples T1, T2, T3, and T4, respectively. The equation of Bosi (2013) [^{W}OH = 2 − 1.01 · BVS(*O*1) − 0.21 − F] was used to estimate the ^{W}OH, which was 0.29, 0.30, 0.34, and 0.40 apfu for samples T1, T2, T3, and T4, respectively. Accordingly, the amounts of ^{W}O were retrieved at the end of this procedure.

The presence or absence of Li was determined from FTIR spectra, and the final Li_2O contents were calculated on the assumptions of (T + Y + Z) = 15.00 apfu and there being 31 anions. This procedure was validated by the excellent match between the number of electrons per formula unit (epfu) derived from chemical and structural data (deviations < 0.4 epfu). Site populations for the *X*, *B*, *T*, *O*3 (≡ V anions), and *O*1 (≡ W anions) sites follow the standard site preference for tourmaline (Henry et al., 2011), whereas the *Y* and *Z* site populations were optimized by the procedure of Bosi et al. (2017) and Wright et al. (2000) and by fixing Li and the minor elements Ti, Mn^{2+}, and Zn at the *Y* site. The resulting empirical crystal chemical formulae are reported in Table 2.

In the studied samples, the main substitution is $2Fe^{2+} \leftrightarrow (Al + Li)$, typical of the schorl–elbaite series. Yet the fragments of the multi-coloured crystal examined can be further classified as hydroxy-, fluor- and oxy-species (Henry et al., 2011). According to the empirical crystal chemical formulae, the core fragments T4 and T3 are ^{W}O-rich, F-bearing schorl, whereas the rim fragments T2 and T1 are Fe^{2+}-rich, ^{W}OH-bearing fluor-elbaite (Table 2).

4 Discussion

Based on the results obtained from the four crystal fragments examined here, the multi-coloured, zoned tourmaline crystal from the Cruzeiro pegmatite shows a well-defined chemical evolution from core to rim. In detail, concerning the *X*-site cations, all fragments belong to the alkali group, with Na contents slightly increasing from core to rim paralleled by a vacancy content $^{X}\square$ decrease (Fig. 3a). Concerning the *Y*-site cations, Mg contents are at their maximum in the inner

Table 2. Empirical crystal chemical formulae of the selected fragments of a multi-coloured, zoned tourmaline crystal from the Cruzeiro pegmatite (Minas Gerais, Brazil).

Crystal fragment	Empirical formula
T1	$^{X}(Na_{0.84}\square_{0.14}Ca_{0.02}K_{0.01})_{\Sigma 1.00}\ ^{Y}(Fe^{2+}_{0.78}Al_{1.07}Li_{0.95}Mn^{2+}_{0.15}Mg_{0.02}Zn_{0.01}Ti^{4+}_{0.01})_{\Sigma 3.00}$ $^{Z}Al_{6.00}(^{T}Si_{6.00}O_{18})(^{B}BO_3)_3\ ^{V}(OH)_3\ ^{W}[(OH)_{0.29}F_{0.69}O_{0.02}]_{\Sigma 1.00}$
T2	$^{X}(Na_{0.79}\square_{0.17}Ca_{0.03}K_{0.01})_{\Sigma 1.00}\ ^{Y}(Fe^{2+}_{1.10}Al_{0.99}Li_{0.67}Mn^{2+}_{0.20}Zn_{0.01}Ti^{4+}_{0.01})_{\Sigma 3.00}$ $^{Z}(Al_{5.96}Mg_{0.04})_{\Sigma 6.00}[^{T}(Si_{5.94}Al_{0.06})_{\Sigma 6.00}O_{18}](^{B}BO_3)_3\ ^{V}(OH)_3\ ^{W}[(OH)_{0.30}F_{0.61}O_{0.09}]_{\Sigma 1.00}$
T3*	$^{X}(Na_{0.65}\square_{0.32}Ca_{0.02}K_{0.01})_{\Sigma 1.00}\ ^{Y}(Fe^{2+}_{1.65}Al_{1.15}Fe^{3+}_{0.06}Mn^{2+}_{0.05}Zn_{0.05}Ti^{4+}_{0.04})_{\Sigma 3.00}$ $^{Z}(Al_{5.52}Fe^{2+}_{0.30}Mg_{0.18})_{\Sigma 6.00}[^{T}(Si_{5.87}Al_{0.13})_{\Sigma 6.00}O_{18}](^{B}BO_3)_3\ ^{V}(OH)_3\ ^{W}[(OH)_{0.34}F_{0.28}O_{0.38}]_{\Sigma 1.00}$
T4	$^{X}(Na_{0.67}\square_{0.29}Ca_{0.03}K_{0.01})_{\Sigma 1.00}\ ^{Y}(Fe^{2+}_{1.48}Al_{1.22}Mn^{2+}_{0.02}Mg_{0.21}Zn_{0.03}Ti^{4+}_{0.04})_{\Sigma 3.00}\ ^{Z}(Al_{5.34}Mg_{0.49}$ $Fe^{2+}_{0.11}Fe^{3+}_{0.07})_{\Sigma 6.00}[^{T}(Si_{5.96}Al_{0.04})_{\Sigma 6.00}O_{18}](^{B}BO_3)_3\ ^{V}(OH)_3\ ^{W}[(OH)_{0.40}F_{0.21}O_{0.39}]_{\Sigma 1.00}$

* From Bosi et al. (2015).

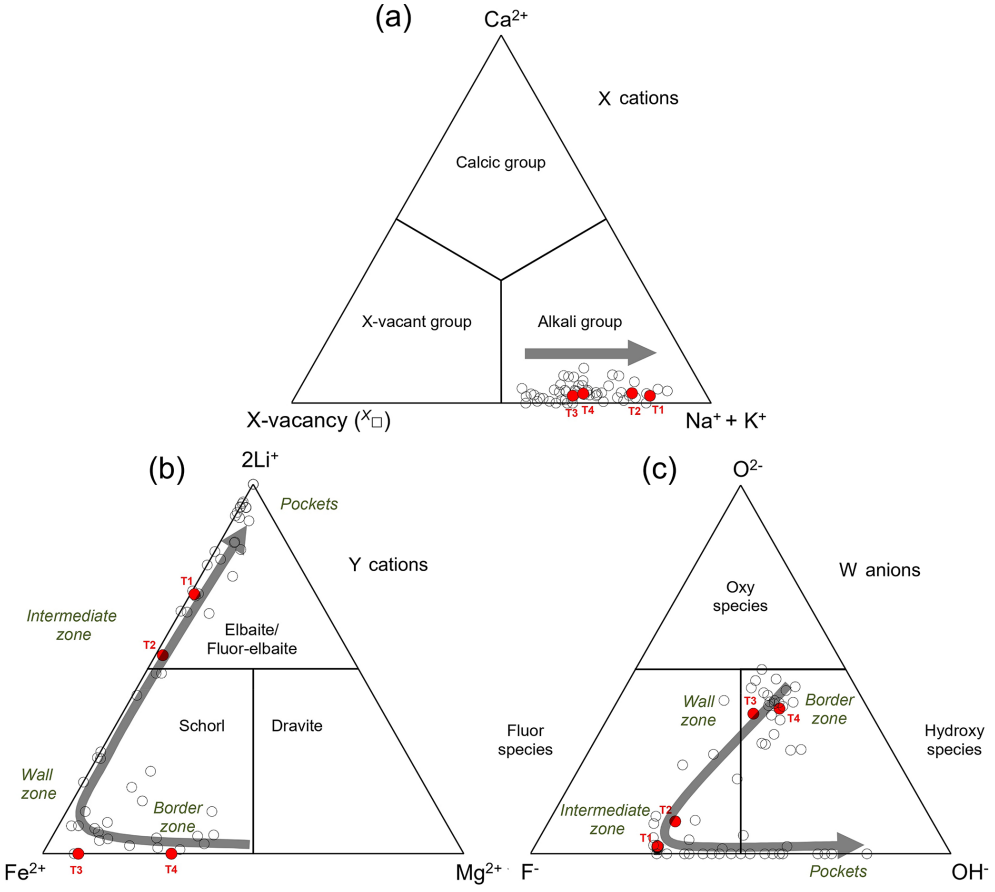

Figure 3. Ternary diagrams for tourmaline illustrating the dominant occupancy at the *X* site **(a)**, at the *Y* site **(b)**, and in terms of W anions **(c)**. Filled red circles: T1, T2, T3, and T4 selected fragments of the multi-coloured, zoned tourmaline crystal studied from the Cruzeiro pegmatite. Empty circles: compositionally homogeneous crystals occurring in the various zones of the Cruzeiro pegmatite (from Federico et al., 1998). The grey arrows represent the evolutionary compositional trend from the border zone to the intermediate zone, pockets included.

core (T4) and strongly decrease from core to rim and Fe^{2+} reaches a maximum in the outer core (T3) and then significantly drops in the rim, whereas Li is almost zero in the core and then significantly rises in the rim (Fig. 3b). With reference to W anions, OH contents are at their maximum in the core (with T4 > T3), even though they are also relatively

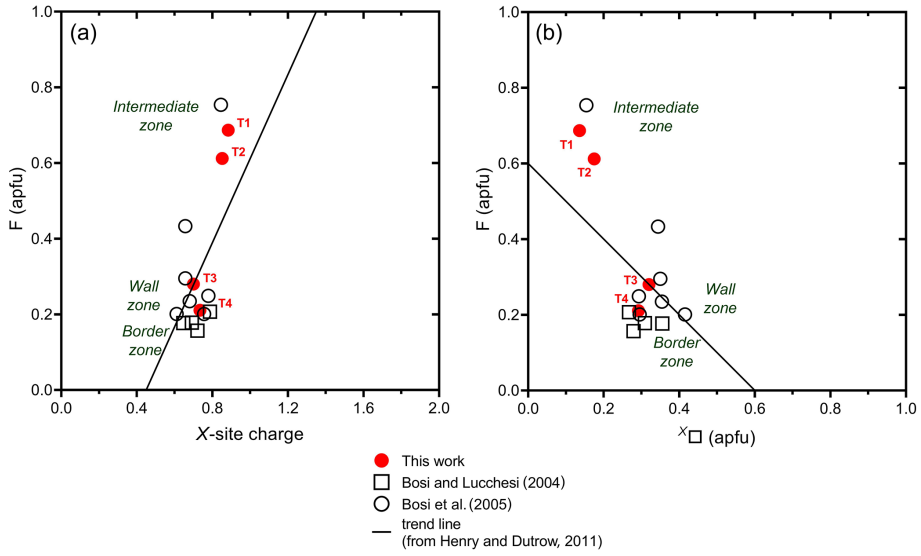

Figure 4. Binary plots showing the relations of F content (apfu) with **(a)** X-site charge, and **(b)** X-site vacancy ($^{X}\square$) (apfu) for tourmalines from the Cruzeiro pegmatite (pockets excluded). The solid lines represent the reference trend lines reported by Henry and Dutrow (2011).

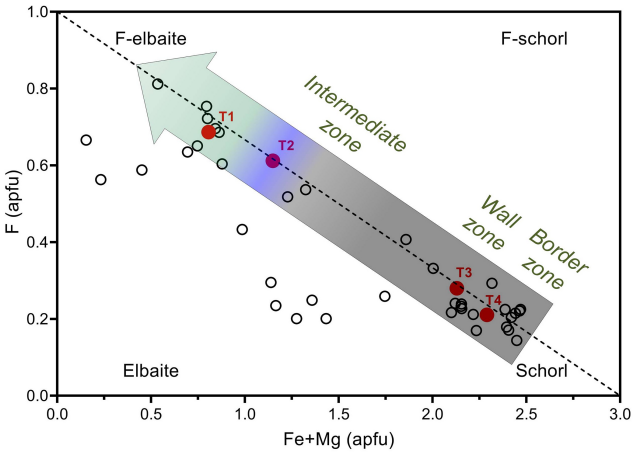

Figure 5. Distribution of tourmalines from the Cruzeiro pegmatite on the F–(Fe^{2+} + Mg) diagram. Filled red circles represent selected fragments of the studied multi-coloured, zoned crystal. The three-band-coloured arrow provides a visual representation of the colour change observed in the studied crystal fragments. Empty circles represent compositionally homogeneous crystals occurring in the various zones of the Cruzeiro pegmatite (pockets excluded). The dashed line represents the ideal $F = 1 - 0.33(Fe^{2+} + Mg)$ relation (with $Mg \ll Fe$).

high in the rim. The main difference between the two regions is that in the core the ^{W}OH contents are almost paired by ^{W}O contents, whereas in the rim the ^{W}OH contents are doubled by ^{W}F contents (Fig. 3c).

Based on a global database of tourmaline compositions, Henry and Dutrow (2011) identified a positive correlation of F contents with X-site charge and a negative correlation with $^{X}\square$. Fluorine contents of the fragments studied generally follow the same trends, increasing from core to rim (Fig. 4a, b).

Moreover, the increase in F contents is negatively correlated with Fe^{2+} contents, as approximated by the equation $F = 1 - 0.33Fe^{2+}$ (in apfu), and the observed correlation improves even further when the minor amounts of Mg in the schorl samples are added to Fe^{2+} contents (Fig. 5).

The negative correlation between Fe^{2+} and F could be attributed to the Fe^{2+}–F avoidance in silicates, for which Fe^{2+} tends to avoid F-coordinated sites (Rosenberg and Foit, 1977). However, Boukili et al. (2002) have shown that the Fe^{2+}–F avoidance rule may not play the determining role in the F content of the micas that is generally agreed upon, and the occurrence of fluorannite, $KFe^{2+}_3(Si_3Al)O_{10}F_2$ (Shen et al., 2000), aligns with this hypothesis. A similar conclusion is also supported by the occurrence of fluor-schorl, $NaFe^{2+}_3Al_6Si_6O_{18}(BO_3)_3(OH)_3F$, in granitic pegmatites (Jolliff et al., 1986; Ertl et al., 2016).

At Cruzeiro – owing to the absence of contamination of the pegmatitic melt by the quartzite host rock – the observed increase in F in tourmalines throughout the pegmatite up to the intermediate zone could be attributed to progressively greater F concentration in the residual melt during pegmatite crystallization. Notably, a very similar trend is also shown by other granitic pegmatites worldwide (Fig. 6).

In the same figure (Fig. 6) it appears that, after a peak in fluor-elbaite, F content drops in elbaitic crystals grown within (or close to) miarolitic pockets. Besides crystallization of F-bearing phases in the inner zones of the pegmatites that depleted the melt of F, the observed drop is likely due to the typical partitioning behaviour of F in the presence of aqueous fluid and silicate melt, for which F preferentially re-

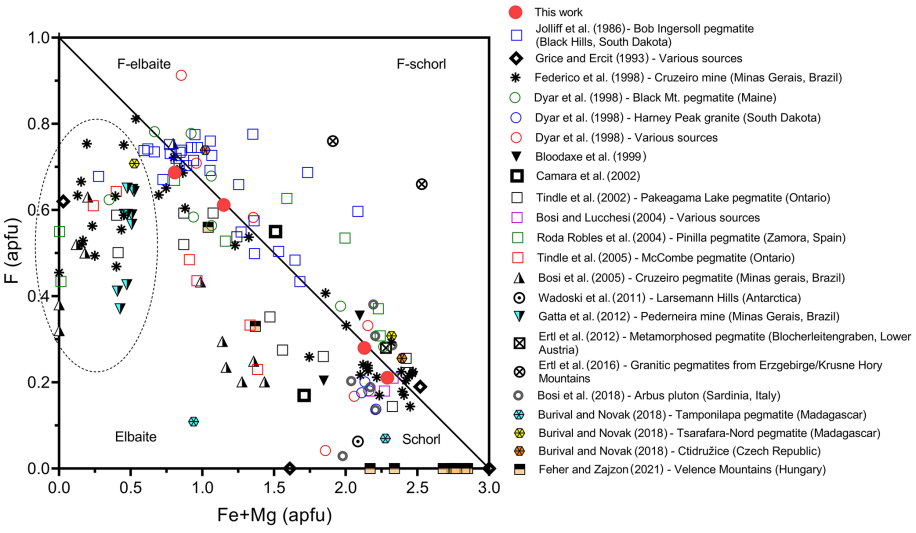

Figure 6. Distribution of compositions of tourmalines found in uncontaminated granitic pegmatites in the F–(Fe^{2+} + Mg) diagram. The samples contained in the region outlined by the dashed line are fluor-elbaite and elbaite crystals grown within (or close to) miarolitic pockets. The solid line represents the $F = 1 - 0.33(Fe^{2+} + Mg)$ relation (with $Mg \ll Fe$).

mains in the melt (Hards, 1976; Fuge, 1977; Burnham, 1979; Manning, 1981; Jolliff et al., 1986).

5 Conclusions

Cruzeiro tourmalines exhibit overlapping compositions between the core–rim-zoned tourmalines and the homogeneous tourmalines found along the pegmatite, from outer to inner zones. Consequently, the initial hypothesis – i.e. that the chemical variations recorded by the multi-coloured, zoned tourmaline crystal reflect the compositional evolution experienced by the homogeneous tourmalines during the pegmatite differentiation – is fully supported. In particular, the presence of maximum Mg content in the black inner core of the zoned crystal closely matches the composition of the homogeneous black dravite-rich schorl occurring in the border and wall zones of Cruzeiro. Likewise, the presence of maximum Fe^{2+} content in the black outer core of the zoned crystal closely matches the composition of schorl occurring in the wall and external intermediate zones of Cruzeiro. Similarly, the maximum (Al + Li) and minor Mn observed in the blue–green rim of the zoned crystal closely match the composition of the homogeneous blue and green fluor-elbaite occurring in the internal intermediate zone, where the multi-coloured, zoned crystal was collected. Furthermore, the chemical evolution of both the zoned crystal and the homogeneous crystals reflects the ideal covariation of cation distribution at the tourmaline *Y*-site in response to decreasing temperature and increasing fractionation of the melt (Jolliff et al., 1986).

Tourmaline is well known for its ability to record environmental changes (e.g. Dutrow and Henry, 2011). The Cruzeiro granitic pegmatite provides a fascinating example of this phenomenon. Overall, the parallel evolution of zoned and homogeneous tourmalines from the same pegmatite reveals that a zoned tourmaline, observed at the scale of single crystals, can record and document not only its growth history, but also the chemical evolution of its host pegmatite, effectively storing the information within its multi-coloured zones and preserving it through time. Moreover, in uncontaminated granitic pegmatite systems such as that of Cruzeiro, the compositional evolution of tourmaline actually progresses from schorl to fluor-elbaite, rather than directly from schorl to elbaite. Notably, the decrease in Fe coupled with the increase in F up to the fluor-elbaite holds for both the multi-coloured chemically zoned and the homogeneous tourmaline crystals across the pegmatites. After the F peak, OH-rich fluor-elbaite and elbaite eventually crystallize only where H_2O-rich environments occur (e.g. within miarolitic pockets formed after the exsolution of an aqueous fluid prior to complete pegmatite solidification).

Data availability. Mossbauer spectroscopy data as well as X-ray diffraction data and FTIR and OAS spectra are available in the Supplement.

Supplement. The supplement related to this article is available online at: https://doi.org/10.5194/ejm-37-1-2025-supplement.

Author contributions. The starting material was characterized by CG, GBA, FB, HS, and UH; data validation and merging were performed by CG, GBA, and FB; discussion of results and

manuscript preparation were carried out by the whole research team.

Competing interests. The contact author has declared that none of the authors has any competing interests.

Disclaimer. Publisher's note: Copernicus Publications remains neutral with regard to jurisdictional claims made in the text, published maps, institutional affiliations, or any other geographical representation in this paper. While Copernicus Publications makes every effort to include appropriate place names, the final responsibility lies with the authors.

Special issue statement. This article is part of the special issue "Celebrating the outstanding contribution of Paola Bonazzi to mineralogy". It is not associated with a conference.

Acknowledgements. This article is in memory of Paola Bonazzi, whose example of scientific integrity and dedication will always be an inspiration. The authors thank Darrell Henry and Vincent van Hinsberg for their useful comments that stimulated a revision of the first version and the chief editor Elisabetta Rampone and associate editor Luca Bindi for their efficient handling of the manuscript. The authors wish to extend their gratitude to Marcello Serracino (CNR–IGAG, Rome) for his kind assistance during EMP analyses.

Financial support. This research was supported by grants of the Italian Ministero dell'Istruzione, dell'Università e della Ricerca (PRIN 2020 "HYDROX – HYDRous- vs. OXo-components in minerals: adding new pieces to the Earth's H2O cycle puzzle", project no. 2020WYL4NY) and of the Sapienza University of Rome (Progetti Ateneo – Piccoli e Medi 2020, 2021, and 2022) awarded to Ferdinando Bosi and Giovanni B. Andreozzi.

Review statement. This paper was edited by Luca Bindi and reviewed by Vincent van Hinsberg and Darrell Henry.

References

Altieri, A., Pezzotta, F., Skogby, H., Hålenius, U., and Bosi, F.: Blue growth zones caused by Fe^{2+} in tourmaline crystals from the San Piero in Campo gem-bearing pegmatites, Elba Island, Italy, Mineral. Mag., 86, 910–919, https://doi.org/10.1180/mgm.2022.101, 2022.

Andreozzi, G. B., Ottolini, L., Lucchesi, S., Graziani, G., and Russo, U.: Crystal chemistry of the axinite-group minerals: A multi-analytical approach, Am. Mineral., 85, 698–706, https://doi.org/10.2138/am-2000-5-607, 2000.

Andreozzi, G. B., Lucchesi, S., Graziani, G., and Russo, U.: Site distribution of Fe^{2+} and Fe^{3+} in the axinite mineral group: New crystal-chemical formula, Am. Mineral., 89, 1763–1771, https://doi.org/10.2138/am-2004-11-1223, 2004.

Andreozzi, G. B., Bosi, F., and Longo, M.: Linking Mössbauer and structural parameters in elbaite-schorl-dravite tourmalines, Am. Mineral., 93, 658–666, 2008.

Berryman, E. J., Wunder, B., Ertl, A., Koch-Müller, M., Rhede, D., Scheidl, K., Giester, G., and Heinrich, W.: Influence of the X-site composition on tourmaline's crystal structure: Investigation of synthetic K-dravite, dravite, oxy-uvite, and magnesio-foitite using SREF and Raman spectroscopy, Phys. Chem. Miner., 43, 83–102, https://doi.org/10.1007/s00269-015-0776-3, 2016.

Bilal, E., César-Mendes, J., Correia-Neves, J. M., and Nasraoui, M.: Chemistry of some pegmatites of São José da Safira area, Minas Gerais, Brazil, Rev. Rom. Mat., 78, 4–6, 1997.

Bilal, E., César-Mendes, J., Correia-Neves, J. M., Nasraoui, M., and Fuzikawa, K.: Chemistry of tourmalines in some pegmatites of São José da Safira area, Minas Gerais, Brazil. J. Geosci., 43, 33–38, 1998.

Bloodaxe, E. S., Hughes J. M., Dyar, M. D., Grew, E. S., and Guidotti, C. V.: Linking structure and chemistry in the Schorl-Dravite series, Am. Min., 84, 922–929, 1999.

Bosi, F.: Bond-valence constraints around the $O1$ site of tourmaline, Mineral. Mag., 77, 343–351, https://doi.org/10.1180/minmag.2013.077.3.08, 2013.

Bosi, F. and Lucchesi, S.: Crystal chemistry of the schorl-dravite series, Eur. J. Mineral., 16, 335–344, https://doi.org/10.1127/0935-1221/2004/0016-0335, 2004.

Bosi, F. and Lucchesi, S.: Crystal chemical relationships in the tourmaline group: Structural constraints on chemical variability, Am. Mineral., 92, 1054–1063, https://doi.org/10.2138/am.2007.2370, 2007.

Bosi, F., Andreozzi, G. B., Federico, M., Graziani, G., and Lucchesi, S.: Crystal chemistry of the elbaite-schorl series, Am. Mineral., 90, 1784–1792, https://doi.org/10.2138/am.2005.1827, 2005.

Bosi, F., Andreozzi, G. B., Skogby, H., Lussier, A. J., Yassir, A., and Hawthorne, F. C.: Fluor-elbaite, $Na(Li_{1.5}Al_{1.5})Al_6(Si_6O_{18})(BO_3)_3(OH)_3F$, a new mineral species of the tourmaline supergroup, Am. Mineral., 98, 297–303, https://doi.org/10.2138/am.2013.4285, 2013.

Bosi, F., Andreozzi, G. B., and Skogby, H.: Experimental evidence for partial Fe^{2+} disorder at the Y and Z sites of tourmaline: a combined EMP, SREF, MS, IR and OAS study of schorl, Mineral. Mag., 79, 515–528, https://doi.org/10.1180/minmag.2015.079.3.01, 2015.

Bosi, F., Reznitskii, L., Hålenius, U., and Skogby, H.: Crystal chemistry of Al-V-Cr oxy-tourmalines from Sludyanka complex, Lake Baikal, Russia, Eur. J. Mineral., 29, 457–472, https://doi.org/10.1127/ejm/2017/0029-2617, 2017.

Bosi, F., Naitza, S., Skogby, H., Secchi, F., Conte, A. M., Cuccuru, S., Hålenius, U., De La Rosa, N., Kristiansson, P., Nilsson, E. J. C., Ros, L., and Andreozzi, G. B.: Late magmatic controls on the origin of schorlitic and foititic tourmalines from late-Variscan peraluminous granites of the Arbus pluton (SW Sardinia, Italy): Crystal-chemical study and petrological constraints, Lithos, 308–309, 395–411, https://doi.org/10.1016/j.lithos.2018.02.013, 2018.

Boukili, B., Holtz, F., Robert, J. L., and Beny, J. M.: "Fe–F avoidance rule" in ferrous-aluminous (OH,F) biotites, Schweiz-

erische mineralogisch petrographisches Mitteilungen, 82, 549–559, 2002.

Brown, I. D. and Altermatt, D.: Bond-valence parameters obtained from a systematic analysis of the Inorganic Crystal Structure Database, Acta Crystallogr. B, 41, 244–247, 1985.

Buřival, Z. and Novák, M.: Secondary blue tourmaline after garnet from elbaite-subtype pegmatites; implications for source and behavior of Ca and Mg in fluids, J. Geosci., 63, 111–122, https://doi.org/10.3190/jgeosci.257, 2018.

Burnham, C. W.: Magmas and hydrothermal fluids, in: Geochemistry of Hydrothermal Ore Deposits, 2nd Edn., edited by: Barnes, H. L., Wiley-Interscience, New York, 71–136, 1979.

Cámara, F., Ottolini, L., and Hawthorne, F. C.: Crystal chemistry of three tourmalines by SREF, EMPA, and SIMS, Am. Mineral., 87, 1437–1442, https://doi.org/10.2138/am-2002-1021, 2002.

César-Mendes, J.: Mineralogia e gênese dos pegmatitos turmaliníferos da Mina do Cruzeiro, São Josè da Safira, Minas Gerais, PhD Thesis, Univ. São Paulo, São Paulo, Brazil, 1995 (in Portuguese).

Černý, P.: Rare-element granitic pegmatites. part I: Anatomy and internal evolution of pegmatitic deposits, Geosci. Can., 18, 49–67, 1991.

Černý, P. and Ercit, T. S.: The classification of granitic pegmatites revisited, Can. Mineral., 43, 2005–2026, https://doi.org/10.2113/gscanmin.43.6.2005, 2005.

Černý, P., London, D., and Novak, M.: Granitic pegmatites as reflections of their sources, Elements, 8, 289–294, https://doi.org/10.2113/gselements.8.4.289, 2012.

de Mello, F. M. and Bilal, E.: Ages constraints in pegmatite province related to charnockitic host rocks in Minas Gerais, Brazil, Rev. Rom. Mat., 85, 94–98, 2012.

Dutrow, B. L. and Henry, D. J.: Complexly zoned fibrous tourmaline, Cruzeiro mine, Minas Gerais, Brazil: A record of evolving magmatic and hydrothermal fluids, Can. Mineral., 38, 131–143, https://doi.org/10.2113/gscanmin.38.1.131, 2000.

Dutrow, B. L. and Henry, D. J.: Tourmaline: A geologic DVD, Elements, 7, 301–306, https://doi.org/10.2113/gselements.7.5.301, 2011.

Dyar, M. D., Taylor, M. E., Lutz, T. M., Francis, C. A., Guidotti, C. V., and Wise, M.: Inclusive chemical characterization of tourmaline: Mössbauer study of Fe valence and site occupancy, Am. Mineral., 83, 848–864, https://doi.org/10.2138/am-1998-7-817, 1998.

Ertl, A., Schuster, R., Hughes, J. M., Ludwig, T., Meyer, H.-P., Finger, F., Dyar, M. D., Ruschel, K., Rossman, G. R., Klötzli, U., Brandstätter, F., Lengauer, C. L., and Tillmanns, E.: Li-bearing tourmalines in Variscan granitic pegmatites from the Moldanubian nappes, Lower Austria, Eur. J. Mineral., 24, 695–715, https://doi.org/10.1127/0935-1221/2012/0024-2203, 2012.

Ertl, A., Kolitsch, U., Dyar, M. D., Meyer, H.-P., Henry, D. J., Rossman, G.R., Prem, M., Ludwig, T., Nasdala, L., Lengauer, C. L., Tillmanns, E., and Niedermayr, G.: Fluor-schorl, a new member of the tourmaline supergroup, and new data on schorl from the cotype localities, Eur. J. Mineral., 28, 163–177, https://doi.org/10.1127/ejm/2015/0027-2501, 2016.

Federico, M., Andreozzi, G. B., Lucchesi, S., Graziani, G., and Cesar-Mendes, J.: Crystal chemistry of tourmalines. I. Chemistry, compositional variations and coupled substitutions in the pegmatite dikes of the Cruzeiro mine, Minas Gerais, Brazil, Can. Mineral., 36, 415–431, 1998.

Fehér, B. and Zajzon, N.: Tourmalines of the Velence Granite Formation and the surrounding contact slate, Velence Mountains, Hungary, Central European Geology, 64, 38–58, https://doi.org/10.1556/24.2021.00005, 2021.

Fuge, R.: On the behavior of fluorine and chlorine during magmatic differentiation, Contrib. Mineral. Petr., 61, 245–249, 1977.

Gatta, G. D., Danisi, R. M., Adamo, I., Meven, M., and Diella, V.: A single-crystal neutron and X-ray diffraction study of elbaite, Phys. Chem. Miner., 39, 577–588, https://doi.org/10.1007/s00269-012-0513-0, 2012.

Gebert, W. and Zemann, J.: Messung des Ultrarot-Pleochroismus von Mineralen II. Der Pleochroismus der OH-Streckfrequenz in Turmalin, Neues Jb. Miner. Monat., 8, 232–235, https://doi.org/10.1007/BF01081565, 1965.

Gonzalez-Carreño, T., Fernandez, M., and Sanz, J.: Infrared and electron microprobe analysis in tourmalines, Phys. Chem. Miner., 15, 452–460, https://doi.org/10.1007/BF00311124, 1988.

Grice, J. D. and Ercit, T. S.: Ordering of Fe and Mg in the tourmaline crystal structure: the correct formula, Neues Jb. Miner. Abh., 165, 245–266, 1993.

Gysi, A. P. and Williams-Jones, A. E.: Hydrothermal mobilization of pegmatite-hosted REE and Zr at Strange Lake, Canada: a reaction path model, Geochim. Cosmochim. Ac., 122, 324–352, https://doi.org/10.1016/j.gca.2013.08.031, 2013.

Hards, N. J.: Distribution of elements between the fluid phase and silicate melt phase of granites and nepheline syenites, Progress in experimental petrology, Nat. Env. Res. Council Publ. Ser., 3, 88–90, 1976.

Henry, D. J. and Dutrow, B. L.: The incorporation of fluorine in tourmaline: Internal crystallographic controls or external environmental influences?, Can. Mineral., 49, 41–56, https://doi.org/10.3749/canmin.49.1.41, 2011.

Henry, D. J., Novák, M., Hawthorne, F. C., Ertl, A., Dutrow, B., Uher, P., and Pezzotta, F.: Nomenclature of the tourmaline supergroup minerals, Am. Mineral., 96, 895–913, https://doi.org/10.2138/am.2011.3636, 2011.

Krivovichev, S.: Structural complexity of minerals: Information storage and processing in the mineral world, Mineral. Mag., 77, 275–326, https://doi.org/10.1180/minmag.2013.077.3.05, 2013.

Jolliff, B. L., Papike, J. J., and Shearer, C. K.: Tourmaline as a recorder of pegmatite evolution: Bob Ingersoll Pegmatite, Black Hills, South Dakota, Am. Mineral., 71, 472–500, 1986.

Lagarec, K. and Rancourt, D. G.: RECOIL. Mössbauer spectral analysis software for Windows, version 1.0, Department of Physics, University of Ottawa, Canada, 1998.

Lima, J. L., Scholz, R., Lana, C., Queiroga, G., and de Castro, M. P.: Mica and tourmaline geochemistry of pegmatites from Conselheiro Pena Pegmatite District, Minas Gerais, Brazil: Implications for pegmatite genesis and economic potential, Geochem. J., 53, 151–170, https://doi.org/10.2343/geochemj.2.0556, 2019.

Linnen, R. L., Van Lichtervelde, M., and Cerný, P.: Granitic pegmatites as sources of strategic metals, Elements, 8, 275–280, https://doi.org/10.2113/gselements.8.4.275, 2012.

London, D.: Granitic pegmatites: an assessment of current concepts and directions for the future, Lithos, 80, 281–303, https://doi.org/10.1016/j.lithos.2004.02.009, 2005.

London, D.: A petrologic assessment of internal zonation in granitic pegmatites, Lithos, 74–104, https://doi.org/10.1016/j.lithos.2013.10.025, 2014.

London, D.: Ore-forming processes within granitic pegmatites, Ore Geol. Rev., 101, 349–383, https://doi.org/10.1016/j.oregeorev.2018.04.020, 2018.

Lussier, A. J. and Hawthorne, F. C.: Oscillatory zoned liddicoatite from Anjanabonoina, central Madagascar. II. Compositional variation and mechanisms of substitution, Can. Mineral., 49, 89–104, https://doi.org/10.3749/2200026, 2011.

Lussier, A. J., Abdu, Y., Hawthorne, F. C., Michaelis, V. K., Aguiar, P. M., and Kroeker, S.: Oscillatory zoned liddicoatite from Anjanabonoina, central Madagascar. I. Crystal chemistry and structure by SREF and 11B and 27Al MAS NMR spectroscopy, Can. Mineral., 49, 63–88, https://doi.org/10.3749/canmin.49.1.63, 2011.

Manning, D. A. C.: The effect of fluorine on liquidus phase relationships in the system Qz-Ab-Or with excess water at 1 Kb, Contrib. Mineral. Petr., 76, 206–215, 1981.

Martin, R. F. and De Vito, C.: The patterns of enrichment in felsic pegmatites ultimately depend on tectonic setting, Can. Mineral., 43, 2027–2048, 2005.

Mattson, S. M. and Rossman, G. R.: Fe^{2+}-Fe^{3+} interactions in tourmaline, Phys. Chem. Miner., 14, 163–171, https://doi.org/10.2113/gscanmin.43.6.2027, 1987.

Novák, M., Škoda, R., Gadas, P., Krmíček, L., and Černý, P.: Contrasting origins of the mixed (NYF + LCT) signature in granitic pegmatites, with examples from the Moldanubian Zone, Czech Republic, Can. Mineral., 50, 1077–1094, https://doi.org/10.3749/canmin.50.4.1077, 2012.

Pouchou, J. L. and Pichoir, F.: Quantitative analysis of homogeneous or stratified microvolumes applying the model "PAP", in: Heinrich, K. F. J. and Newbury, D. E., Electron Probe Quantitation, Plenum, New York, 31–75, https://doi.org/10.1007/978-1-4899-2617-3_4, 1991.

Roda-Robles, E., Pesquera, A., Gil, P. P., Torres-Ruiz, J., and Fontan, F.: Tourmaline from the rare-element Pinilla pegmatite, (Central Iberian Zone, Zamora, Spain): chemical variation and implications for pegmatitic evolution, Mineral. Petr., 81, 249–263, https://doi.org/10.1007/s00710-004-0042-8, 2004.

Rosenberg, P. E. and Foit Jr., F. F.: Fe^{2+}-F avoidance in silicates, Geochim. Cosmochim. Ac., 41, 345–346, 1977.

Shaw, R. A., Goodenough, K. M., Roberts, N. M. W., Horstwood, M. S. A., Chenery, S. R., and Gunn, A. G.: Petrogenesis of rare-metal pegmatites in high-grade metamorphic terranes: a case study from the Lewisian Gneiss Complex of north-west Scotland, Precambrian Res., 281, 338–362, https://doi.org/10.1016/j.precamres.2016.06.008, 2016.

Shen, G., Lu, Q., and Xu, J.: Fluorannite: A new mineral of the mica group from the western suburb of Suzhou City, Ac. Petrol. Mineral., 19, 355–362, 2000 (in Chinese, English absract).

Simmons, W. B. and Webber, K. L.: Pegmatite genesis: state of the art, Eur. J. Mineral. 20, 421–438, https://doi.org/10.1127/0935-1221/2008/0020-1833, 2008.

Skogby, H., Bosi, F., and Lazor, P.: Short-range order in tourmaline: a vibrational spectroscopic approach to elbaite, Phys. Chem. Miner., 39, 811–816, https://doi.org/10.1007/s00269-012-0536-6, 2012.

Sheldrick, G. M.: Crystal structure refinement with SHELXL, Acta Crystallogr. C, 71, 3==8, 2015.

Tindle, A. G., Breaks, F. W., and Selway, J. B.: Tourmaline in petalite-subtype granitic pegmatites: evidence of fractionation and contamination from the Pakeagama Lake and Separation Lake areas of northwestern Ontario, Canada, Can. Mineral., 40, 753–788, https://doi.org/10.2113/gscanmin.40.3.753, 2002.

Tindle, A. G., Selway, J. B., and Breaks, F. W.: Liddicoatite and associated species from the McCombe spodumene-subtype rare-element granitic pegmatite, northwestern Ontario, Canada, Can. Mineral., 43, 769–793, https://doi.org/10.2113/gscanmin.43.2.769, 2005.

van Hinsberg, V. J., Henry, D. J., and Dutrow, B. L.: Tourmaline as a petrologic forensic mineral: A unique recorder of its geologic past, Elements, 7, 327–332, https://doi.org/10.2113/gselements.7.5.327, 2011.

Wadoski, E. R., Grew, E. S., and Yates, M. G.: Compositional evolution of tourmaline-supergroup minerals from granitic pegmatites in the Larsemann Hills, East Antarctica, Can. Mineral., 49, 381–405, https://doi.org/10.3749/canmin.49.1.381, 2011.

Watenphul, A., Burgdorf, M., Schlüter, J., Horn, I., Malcherek, T., and Mihailova, B.: Exploring the potential of Raman spectroscopy for crystallochemical analyses of complex hydrous silicates: II. Tourmalines, Am. Mineral., 101, 970–985, https://doi.org/10.2138/am-2016-5530, 2016.

Wright, S. E., Foley, J. A., and Hughes, J. M.: Optimization of site occupancies in minerals using quadratic programming, Am. Mineral., 85, 524–531, https://doi.org/10.2138/am-2000-0414, 2000.